

Journal of Hydrodynamics, Ser. B, 2005, 17(1): 12 - 21
China Ocean Press, Beijing - Printed in China

NUMERICAL EXPERIMENTS OF THREE DIMENSIONAL MIXING OF NATURAL GAS AND AIR*

XU Sheng-li

Department of Mechanics and Mechanical Engineering, University of Science and Technology of China, Hefei 230026, China, e-mail: slxu@ustc.edu.cn

LIU Kai

Technical Center of Diesel Engines of Shanghai Limited Corporation, Shanghai 200042, China

ZHU Zuo-jin

Institute of Engineering Science, University of Science and Technology of China, Hefei 230026, China

YUE Peng-tao

Department of Mechanics and Mechanical Engineering, University of Science and Technology of China, Hefei 230026, China

(Received Nov. 12, 2003)

ABSTRACT: This study presents the numerical results for the three-dimensional natural gas-air mixing in a rectangular subsonic channel under the standard datum state. The lower and upper decomposition method was employed to obtain the solutions of the full Navier-Stokes equations capable of describing compressible fluid mixing. Grid was generated by the area orthogonal technique. The results indicate that three-dimensional mixing between Natural Gas (NG) and air has more complicated compressible waves around the injection nozzle. The presence of injection with large speed can suppress the boundary separation happened occurring at the top wall due to the channel expansion, but makes the near-wake flow more complicated. The mixing region can be widened by increasing the injection speed. The recurrence of the vortex structure and the coherent structure can be found from the full Navier-Stokes simulation. It can be concluded that the increase in the injection velocity can improve the effectiveness of mixing of NG and air in the near wake of the injectors.

KEY WORDS: fuel-air mixing, LU decomposition, numerical simulation

1. INTRODUCTION

In the recent decades, to meet the requirement of environmental protection, NG has been used extensively as engine fuel in gas pipeline transmission and, more recently, as a fuel for transportation including both light- and heavy-duty vehicles^[1-3]. It was found that the Compressed Natural Gas (CNG) has a number of advantages o-

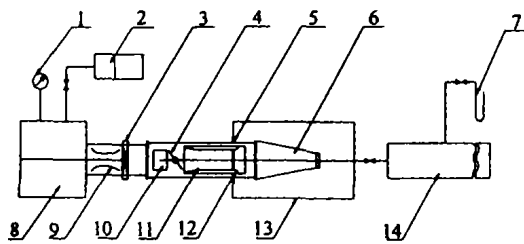
ver gasoline especially for low pollutant emission vehicles^[4].

The objective of the numerical experiments is to comparatively study the effect of NG injection on the mixing patterns in the near wake of the NG nozzle, as shown in Fig. 1. The flow is considered to be fully compressible, so that its flow field can be evaluated by solving the full Navier-Stokes equations that are compatible to most actual flows. To present the results in an apparent manner, and for the convenience of comparison, a two dimensional benchmark flow case is studied to precede the numerical experiment for the three-dimensional NG-air mixing.

There are a number of numerical methods available for the solution of the Navier-Stokes equations. For instance, Patankar^[5] has presented the series of SIMPLE method for heat and fluid flow, Brown et al.^[6] have presented the accurate projection methods for the Navier-Stokes equations, which has been used to study the laminar natural convections in a tall cavity^[7], Le Quere and Roquefort^[8] have presented a Chebyshev polynomial method which has now been used effectively for the analysis of bifurcation of double-diffusive convection with opposing horizontal thermal solutal gradient^[9]. For circular cylinder wake flows

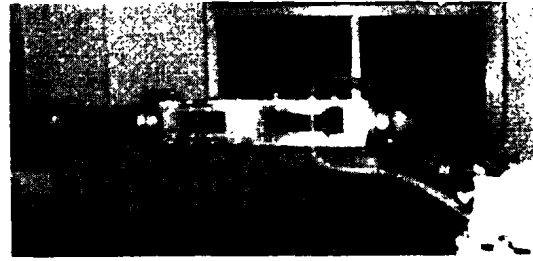
* **Biography:** XU Sheng-li (1965-), Male, Ph. D., Professor

in the sub-critical regime when the Reynolds number Re ranges from 10^3 to 10^4 , three-dimensional numerical simulation with the CFX-4 simulator was carried out by Wang, Liu and Miao^[10]. It was found that at high Reynolds number the effect of three-dimensionality is significant, and three-dimensional simulation outputs smaller hydrodynamic force coefficients. However, in the present study of NG-air mixing, the method proposed by Shuen^[11] is appreciated the more and employed together with the grid generation technique-Area Orthogonal (AO) developed by Knupp^[12]. The method of Shuen is grounded on the upwind differencing Lower and Upper (LU) factorization, which was found to be also available in capturing the solutions for supersonic reactive flows^[13]. It should be noted the LU implicit scheme was first used by Yoon and Jameson for high speed inlet analysis^[14] and for the solution of Euler equations^[15]. Evidently, the NG mixing has been involved with turbulence. Instead of large eddy simulation of turbulent flow, we select Direct Navier-Stokes (DNS) simulation for the sake of computational cost. The advantage of DNS is its more convenience to capture the instantaneous motion of vortices near the wake of the NG nozzle.



1(a) Chart view

The following part of the paper contains the section about governing equations, which is followed by the section about numerical method. Then the results and discussion are presented that are prior to the final conclusions.



1(b) Test section

Fig.1 Test rig of NG-air mixing

2. GOVERNING EQUATIONS

The numerical experiments should be able to explore the mixing characteristics between NG and air. But the irregular boundaries of the physical geometry as well as the requirement of multi-species field evaluation have made it difficult for the treatment of the mixing simulation.

To describe the mixing process more accurately, the full N-S equations can be employed to describe the NG-air mixing process in the three-dimensional subsonic rectangular channel. Using the Cartesian coordinate system, the N-S equations for the multi-species system can be written as

$$\frac{\partial U}{\partial t} + \frac{\partial F}{\partial x} + \frac{\partial G}{\partial y} + \frac{\partial H}{\partial z} = \frac{\partial F_v}{\partial x} + \frac{\partial G_v}{\partial y} + \frac{\partial H_v}{\partial z} \quad (1)$$

where the subscript "v" is used for viscous terms. With the superscript "T" denoting the transpose of any matrix, the variable vector and the flux can be written as

$$U = [\rho^1, \rho^2, \dots, \rho^n, \rho u, \rho v, \rho w, \rho E]^T \quad (2a)$$

$$F = [mY^1, mY^2, \dots, mY^n, p + m^2/\rho, mm/\rho, mk/\rho, m(\rho E + p)/\rho]^T \quad (2b)$$

$$G = [nY^1, nY^2, \dots, nY^n, mn/\rho, p + n^2/\rho, nk/\rho, n(\rho E + p)/\rho]^T \quad (2c)$$

$$H = [kY^1, kY^2, \dots, kY^m, km/\rho, kn/\rho,$$

$$p + k^2/\rho, k(\rho E + p)/\rho]^T \quad (2d)$$

which is accompanied by the viscous flux terms given by

$$F_v = [\rho D \frac{\partial Y^1}{\partial x}, \rho D \frac{\partial Y^2}{\partial x}, \dots, \rho D \frac{\partial Y^m}{\partial x},$$

$$\tau_{xx}, \tau_{yy}, \tau_{zz}, u\tau_{xx} + v\tau_{yy} +$$

$$w\tau_{zz} + q_x]^T \quad (3a)$$

$$G_v = [\rho D \frac{\partial Y^1}{\partial y}, \rho D \frac{\partial Y^2}{\partial y}, \dots, \rho D \frac{\partial Y^m}{\partial y},$$

$$\tau_{xy}, \tau_{yy}, \tau_{yz}, u\tau_{xy} + v\tau_{yy} +$$

$$w\tau_{yz} + q_y]^T \quad (3b)$$

$$H_v = [\rho D \frac{\partial Y^1}{\partial z}, \rho D \frac{\partial Y^2}{\partial z}, \dots, \rho D \frac{\partial Y^m}{\partial z},$$

$$\tau_{xz}, \tau_{yz}, \tau_{zz}, u\tau_{xz} + v\tau_{yz} +$$

$$w\tau_{zz} + q_z]^T \quad (3c)$$

where we have defined that $\rho = \sum \rho'$, $m = \rho u$, $n = \rho v$, $k = \rho w$, with $Y^i = \rho^i/\rho$ being the mass fraction of i -th species. $e = -\frac{p}{\rho} + \sum_{i=1}^m Y^i h_i$ is the total energy per unit mass, and the total energy plus the kinematic energy of motion per unit volume can be given by

$$\rho E = \rho e + \frac{m^2 + n^2 + k^2}{2\rho} \quad (4)$$

The enthalpy per unit mass for the i -th species is

$$h_i = \int_{T^0}^T c_{p,i} dT + h_i^0 \quad (5)$$

where the superscript "0" denotes the standard datum state whose temperature and pressure are respectively 298.1K and 1atm. Assume the NG-air mixture can be viewed as ideal gas, and the universal gas constant, the i -th species molecular weight can be denoted by R_u , w_i , respectively, then from

the ideal gas law, we have

$$p = \frac{R_u T \sum \rho^i}{\sum w_i} \quad (6)$$

while the heat flux term in the x direction can be written as

$$q_x = \frac{\mu c_p}{Pr} \frac{\partial T}{\partial x} + \sum_{i=1}^m \rho D h_i \frac{\partial Y^i}{\partial x} \quad (7)$$

Note that similar expressions can be given for the heat flux in the y and z directions. If the Lewis number for the gas mixture is unity, using Pr as the Prandtl number, we have the mass diffusion coefficient $\rho D = \mu/Pr$. The dynamic viscosity can be evaluated by using the Sutherland expression, with the viscous stress written as

$$\tau_{xx} = \frac{2}{3} \mu \left(2 \frac{\partial u}{\partial x} - \frac{\partial v}{\partial y} - \frac{\partial w}{\partial z} \right) \quad (8a)$$

$$\tau_{yy} = \frac{2}{3} \mu \left(2 \frac{\partial v}{\partial y} - \frac{\partial w}{\partial z} - \frac{\partial u}{\partial x} \right) \quad (8b)$$

$$\tau_{zz} = \frac{2}{3} \mu \left(2 \frac{\partial w}{\partial z} - \frac{\partial u}{\partial x} - \frac{\partial v}{\partial y} \right) \quad (8c)$$

$$\tau_{xy} = \tau_{yx} = \mu \left(\frac{\partial u}{\partial y} + \frac{\partial v}{\partial x} \right) \quad (8d)$$

$$\tau_{yz} = \tau_{zy} = \mu \left(\frac{\partial v}{\partial z} + \frac{\partial w}{\partial y} \right) \quad (8e)$$

$$\tau_{xz} = \tau_{zx} = \mu \left(\frac{\partial u}{\partial z} + \frac{\partial w}{\partial x} \right) \quad (8f)$$

The governing equations can be normalized by using the scales for length, velocity, temperature and dynamic viscosity defined by the characteristic length L_0 , the sound speed a_0 , temperature T_0 , and the dynamic fluid viscosity of the inflow air. If the normalized labels for each variable can be removed, the governing equations remains its original form.

To improve the resolution of the solutions in the regions with larger gradients of variables and to deal with the complex geometry, special coordinate transformations $t = \tau$, $x = x(\xi, \eta, \zeta)$, $y = y(\xi, \eta, \zeta)$, $z = z(\xi, \eta, \zeta)$ have been employed in the numerical experiments. In the transformed

curvilinear coordinate system, the dimensionless governing equations can be written as

$$\frac{\hat{U}}{\partial \tau} + \frac{\hat{F}}{\partial \xi} + \frac{\hat{G}}{\partial \eta} + \frac{\hat{H}}{\partial \zeta} = \frac{1}{Re} \cdot \left(\frac{\partial \hat{F}_v}{\partial \xi} + \frac{\partial \hat{G}_v}{\partial \eta} + \frac{\partial \hat{H}_v}{\partial \zeta} \right) \quad (9)$$

where $J = | \partial(\xi, \eta, \zeta) / \partial(x, y, z) |$ is the determinant of the Jacobian matrix for the coordinate transformation, and $\hat{U} = J^{-1}U$,

$$\hat{F} = J^{-1}(\xi_r F + \xi_\eta G + \xi_z H),$$

$$\hat{F}_v = J^{-1}(\xi_r F_v + \xi_\eta G_v + \xi_z H_v) \quad (10a)$$

$$\hat{G} = J^{-1}(\eta_r F + \eta_\eta G + \eta_z H),$$

$$\hat{G}_v = J^{-1}(\eta_r F_v + \eta_\eta G_v + \eta_z H_v) \quad (10b)$$

$$\hat{H} = J^{-1}(\zeta_r F + \zeta_\eta G + \zeta_z H),$$

$$\hat{H}_v = J^{-1}(\zeta_r F_v + \zeta_\eta G_v + \zeta_z H_v) \quad (10c)$$

It should be noted that the thermodynamic properties of the mixture can be found from the JANAF table^[16], according to which, the specific heat and the enthalpy for each species can be evaluated by using the following expressions:

$$\frac{c_p}{R_i} = \sum_{j=0}^l a_{i,j} T^j,$$

$$\frac{h_i}{R_i T} = \sum_{j=1}^5 a_{i,j-1} / j + \frac{a_{i,6}}{T} \quad (11)$$

For which the JANAF table has shown the correlation coefficients used above for specific heat at constant pressure and the enthalpy per unit mass of the mixture.

3. NUMERICAL METHOD

It was reported that LU decomposition method is very effective for the solution of the multi-species non-equilibrium reactive flows^[11,13]. Thus it shall be employed in the present numerical experi-

ments for the NG-air mixing process.

Generally, the spatial intervals $\Delta\xi$, $\Delta\eta$, $\Delta\zeta$ are all set as unity. For the Right-Hand Side (RHS) terms, the convection and diffusion parts were treated explicitly. The explicit convective terms were differenced by the second order Total Variable Diminishing (TVD) scheme^[17], with the diffusion terms differenced by the second order central scheme. However, the first order upwind scheme was used in the treatment of the implicit convective terms. The numerical experiments are characterized by the LU (lower and upper matrix) decomposition for the solution of the variable increment between two temporal steps. In this section, the solution method was briefly described. Details can be found in Ref. [11].

For convenience, we define the three Jacobian matrices associated with the convections in the three directions in the N-S equations as A , B , and C , thus

$$A = \frac{\partial \hat{F}}{\partial \hat{U}}, \quad B = \frac{\partial \hat{G}}{\partial \hat{U}}, \quad C = \frac{\partial \hat{H}}{\partial \hat{U}} \quad (12)$$

Their spectral radii are represented by λ_A , λ_B , λ_C respectively. Suppose γ_A , γ_B , γ_C can take their values with respect to the constraint: $\gamma_A \geq \lambda_A$, $\gamma_B \geq \lambda_B$, $\gamma_C \geq \lambda_C$, and I is the unit matrix, let D_ξ^- , D_η^- , D_ζ^- represent the backward finite differences in the direction given by their subscripts, with D_ξ^+ , D_η^+ , D_ζ^+ denoting forward differences in the relevant direction, by splitting A , B , C as $A = A^- + A^+$, $B = B^- + B^+$, $C = C^- + C^+$. For time step $\Delta\tau$, we have

$$[I + \Delta\tau(D_\xi^- A^+ + D_\xi^+ A^- + D_\eta^- B^+ + D_\eta^+ B^- + D_\zeta^- C^+ + D_\zeta^+ C^-)] \Delta \hat{U} = \Delta\tau \cdot \text{RHS} \quad (13)$$

where, $\Delta \hat{U} = \hat{U}^{n+1} - \hat{U}^n$, and

$$\text{RHS} = \left[-\frac{\partial \hat{F}}{\partial \xi} - \frac{\partial \hat{G}}{\partial \eta} - \frac{\partial \hat{H}}{\partial \zeta} + \frac{1}{Re} \cdot \left(\frac{\partial \hat{F}_v}{\partial \xi} + \frac{\partial \hat{G}_v}{\partial \eta} + \frac{\partial \hat{H}_v}{\partial \zeta} \right) \right]^n \quad (14)$$

Using the LU method to the left hand side of Eq. (13), we have

$$LN^{-1} - [N - \Delta\tau \cdot (A_{i-1,j,k}^- + B_{i,j-1,k}^- + C_{i,j,k-1}^-)] \Delta\hat{U} = \Delta\tau \cdot \text{RHS},$$

$$L = [N + \Delta\tau \cdot (A_{i-1,j,k}^- + B_{i,j-1,k}^- + C_{i,j,k-1}^-)] \quad (15)$$

where, $N = \text{diag}\{1 + \Delta\tau(\gamma_A + \gamma_B + \gamma_C)\}$, is diagonal, and

$$A^\pm = \frac{1}{2}(A \pm \gamma_A I), \quad B^\pm = \frac{1}{2}(B \pm \gamma_B I),$$

$$C^\pm = \frac{1}{2}(C \pm \gamma_C I) \quad (16)$$

Equation (15) can be solved iteratively by with the following procedure:

(1) Evaluate $(\Delta\hat{U})^*$ by solving

$$L(\Delta\hat{U})^* = \Delta\tau \cdot N \cdot \text{RHS} \quad (17a)$$

(2) Evaluate $(\Delta\hat{U})$ by solving

$$[N + \Delta\tau \cdot (A_{i-1,j,k}^- + B_{i,j-1,k}^- + C_{i,j,k-1}^-)] \Delta\hat{U} = \Delta\hat{U}^* \quad (17b)$$

Note that the grid was generated by virtue of the Area Orthogonal (AO) technique^[12].

The initial and boundary conditions are given as follows:

For initial flow field, it is assumed as uniform, or read from an intermediate data file set as specified value corresponding to an engine cylinder. For boundary conditions, the downstream pressure was used to interpolate the variable values at the exhaust section, the variables at inlet section were interpolated with respect to the isentropic flow theory, for grid on the injectors, the interpolation was also used to define the velocity and density, on walls, non-slip condition was given, while on the symmetrical plane, slip condition was chosen. The details can be found in Ref. [18].

4. RESULTS AND DISCUSSION

Numerical experiments were conducted for

two situations: The first was to explore the mixing patterns between the NG and air in a duct simplified by the two dimensional analysis, a semi-circular cylinder was used to approximate the NG injection nozzle in order to decrease the computational amount. The second was used for the simulation of the NG-air mixing patterns in the three-dimensional channel where its cross sectional area is variable along the stream-wise direction. The first situation can be seen as a benchmark problem for which the NG injection velocity has been studied.

Although the LU approximation has improved the computational efficiency obviously, the numerical experiments accomplished on a Pentium IV personal computer for three-dimensional simulation still require the running time of about one week. The objective of the numerical experiment using the full N-S model described in Section 2 is to further explore the intrinsic physical and fluid mechanical mechanism of the NG-mixing for the optimal design of the mixer of NG fueled engines.

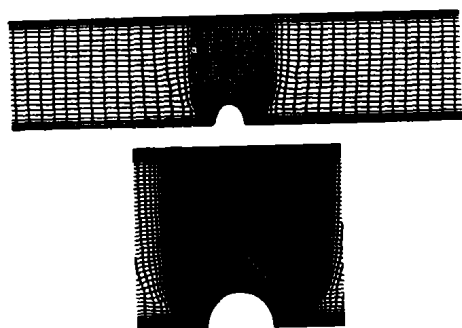
Table 1 Parameters used in the numerical experiments

Case I(2D)	Case II(3D)
Grid: 301 × 101	Grid: 171 × 31 × 65
$T = 298.15\text{K}$	$T = 298.15\text{K}$
$p = 1\text{atm}$	$p = 1\text{atm}$
$v_\infty = 50\text{m/s}$	$v_\infty = 50\text{m/s}$
$v_{mj} = 0, 50, 100\text{m/s}$	$v_{mj} = 0, 100\text{m/s}$

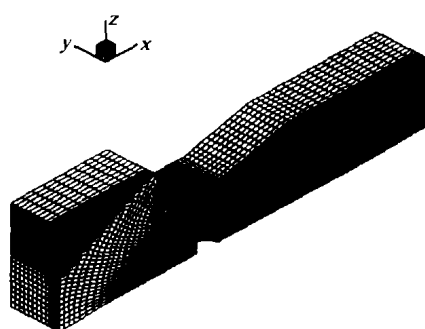
4.1 Parameters used in the numerical experiments

As mentioned in Section 3, the grid generation for the mixing problem is given with the AO technique^[12]. The parameters for the numerical experiments are given in Table 1. It is seen that for the two cases the pressure and temperature are the same as what defined for the standard datum state, i. e. 1atm pressure with the absolute temperature set as 298.15K. The approaching flow velocity is set as 50m/s. The grid number is 301 × 101, with 301 denoting the grid number in the stream-wise direction. On the other hand, the grid number is chosen as 171 × 31 × 65, with 31 and 65 denoting the grids in the y and z direction respectively. The

grids used have been shown in Figs. 2(a) and 2(b) schematically.



2(a) Two-dimensional mixing



2(b) Three-dimensional mixing

Fig. 2 The computational grids

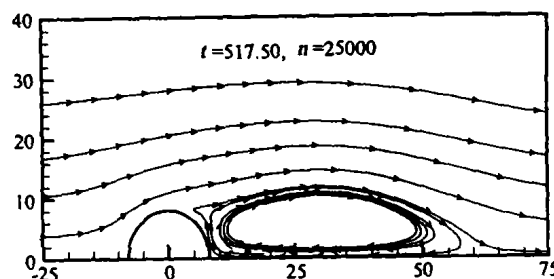
4.2 Solutions with 2D approximation

For the case without injection, Figs. 3(a) and 3(b) has presented the streamlines for two instants: $t = 517.50$, and 539.04 . It is seen that the vortex separated from the semi-cylinder has developed a re-circulation zone, in which flow pressure is lower. The zonal structure is clearly time-dependent.

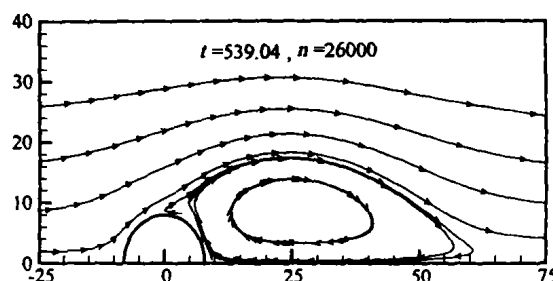
However, when the NG injected at a velocity of 100m/s , the flow field near the wake of the nozzle has been significantly changed. Fig. 4 shows the schematic of the injection position considered in the numerical experiment with NG injection. Fig. 5 shows the contours of the mass fraction of natural gas for 3 instants. Owing to the interference between the NG jets and the air vortices shed from the surface of the NG injectors, the flow patterns have been changed greatly. Recurrence phenomena of the wake flow emerge, and the jets have forced the vortices to move along the downstream direction. During the downstream propagation of vortices, there are the breaking-up and rec-

reation of vortices, which promotes the NG-air mixing.

Correspondingly, the contours of pressure field for the 6 instants are exhibited in Fig. 6. It is seen that the presence of a vortex causes the larger pressure gradient in the wake flow field.



3(a) Without NG injection



3(b) With NG injection

Fig. 3 The streamlines in the near wake of the injection nozzle for two-dimensional mixing

Nevertheless, the detailed flow field is closely related with the injection velocity, which means that the mixing pattern between the natural gas and air may appear to dramatically change as soon as the injection velocity is varied. This is confirmed by the comparison of the mixing pattern shown in Fig. 5 and Fig. 7. In Fig. 7, since the NG injection velocity is 50m/s , the penetration of NG jet in the wake flow becomes shorter than what can be seen in case of 100m/s for the same approaching flow velocity ($= 50\text{m/s}$). Thus the force of displacing the separated vortices decreases, and the NG-air mixing region becomes narrow as compared to the mixing belt seen in Fig. 5. The relevant pressure field for the injection at velocity 50m/s is illustrated in Fig. 8. The comparison of the results obtained with different injection velocities has indicated that the interference between the injection and the wake flow is a key feature in determining the effectiveness of the NG-air mixing.

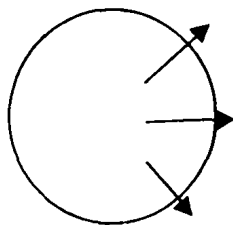


Fig. 4 Schematic of injector at an angle of 45° respected to the horizontal one

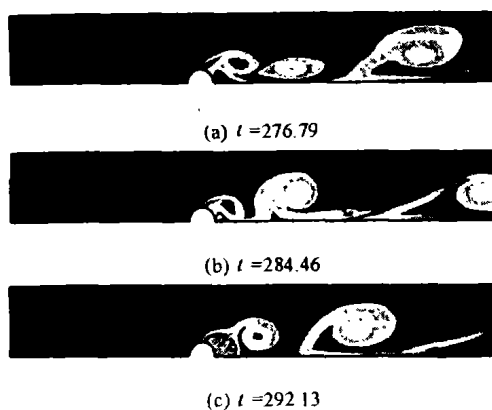


Fig. 5 Mixing patterns shown by density contours of NG at $V_{inj} = 100 \text{ m/s}$

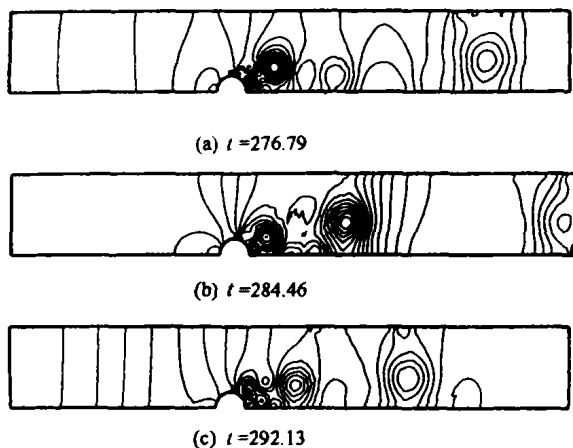


Fig. 6 Pressure contours at $V_{inj} = 100 \text{ m/s}$

4.3 Solutions for three-dimensional mixing

Using the parameters given in the second column of Table 1, the flow field associated with the natural gas-air mixer has been numerically simulated. Fig. 9(a) shows the pressure contours in the three- constant z (see left part) and three-constant y planes (see right part). It is seen that as the result of channel section area variation, for the case

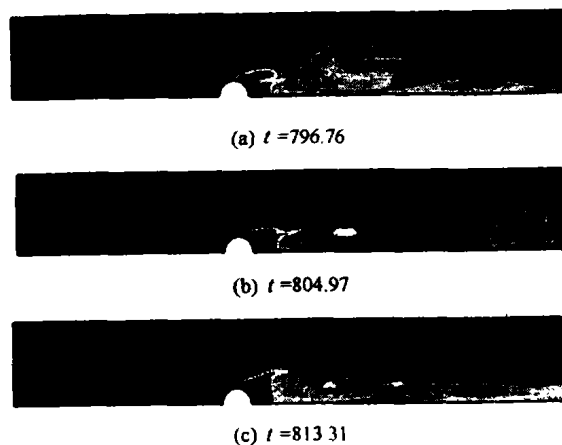


Fig. 7 Mixing patterns shown by density contours of NG at $V_{inj} = 50 \text{ m/s}$

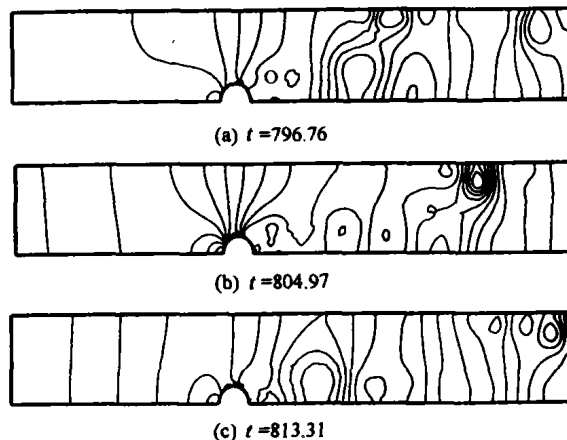


Fig. 8 Pressure contours at $V_{inj} = 50 \text{ m/s}$

of zero injection, in each of the plane illustrated in Fig. 9(a), the distribution of pressure seems to be apparently distinct. For instance, on the upwind surface of the injection nozzle, and on the top wall near the channel convergence portion, there exist dense compressible waves. In particular, larger pressure gradient region has formed by the compressible waves occurred near the stagnation point of the injection nozzle. Compared with the two-dimensional results discussed in the preceding subsection, the pressure waves appearing in the three-dimensional subsonic channel are more complicated.

Figure 10(a) presents the contours of the density field of the NG-air mixed flow in the channel. It is seen that, in the near wake of the injection nozzle and in the channel expansion section, there appear different vortex structures. These vortices are three-dimensional, and hence it is really diff-

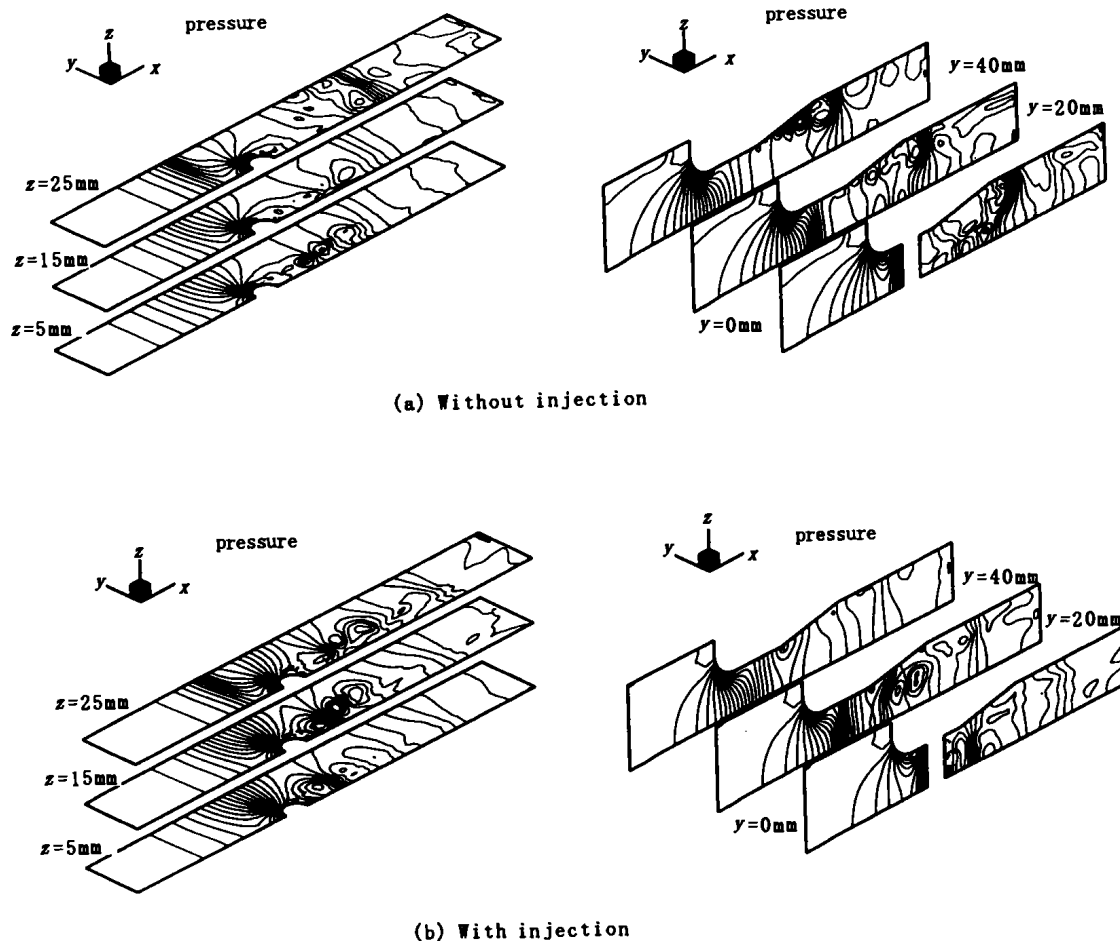


Fig. 9 The pressure contours for three-dimensional flow-field at $V_{mj} = 100\text{m/s}$

icult to present quantitative description. It appears that in the channel expansion section, the vortices are resulted from the boundary separation, which may be caused to the presence of the adverse pressure gradient due to channel expansion. Similar to what has been explored in the two-dimensional situations, on the backwind surface of the injection nozzle, vortex shedding happens, the separated vortices propagate downward during their mutually interaction and evaluation, and coherent structures and recurrence phenomena can be observed.

On the other hand, the presence of the NG injection certainly changes the NG-air mixing and the flow field significantly, as shown in Fig.9(b). At first, it can be seen that the injection has weakened the compressible waves appearing on the top wall, and it also suppresses the boundary layer separation which may affect the NG-air mixing nega-

tively. Secondly, due to interaction between the vortex shedding process and the NG jets from the three column multi-hole nozzle (the total number of holes is 18, with 6 holes per column), the near-wake flow has become more complicated, and so are the compressible waves around the nozzle. These effects from the NG injection can also be seen from the density contours shown in Figs. 10 (b).

Figure 11 depicts the distribution of the equivalence ratio of the NG-air mixed flow for the instant $t = 767.86$ at the exhaust section. Apart from in the right bottom corner region, the NG has dispersed in the remained portion of the channel section. However, the emergence of the sufficiently mixed region is closely related with the vortex motion in the NG-air mixed flow.

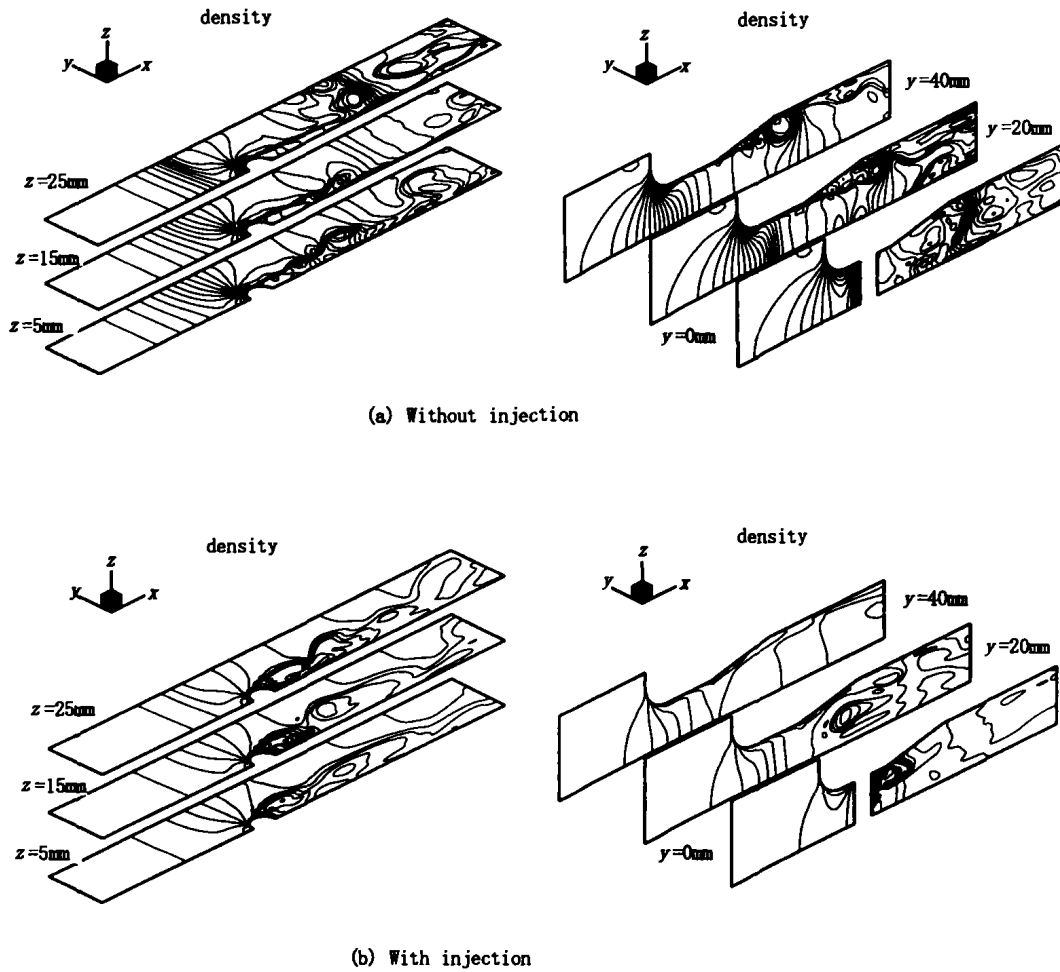


Fig. 10 The density contours for three-dimensional flow-field at $V_{inj} = 100\text{m/s}$

5. CONCLUSIONS

This paper has presented the numerical experiments with the full N-S model for the three-dimensional NG-air mixing in subsonic channel under the standard datum state. It indicates that the model is capable of providing physically true mixing patterns not only in the case of the benchmark problem for which two-dimensional approximation was employed, but also in the case of real three-dimensional NG-air mixed flow in the subsonic channel under the conditions close to the case visualized by Schlieren method.

The numerical method in these experiments has combined the LU decomposition with the AO grid generation. The results based on this method have indicated that three-dimensional mixing between NG and air has more complicated compressible waves around the injection nozzle. The pres-

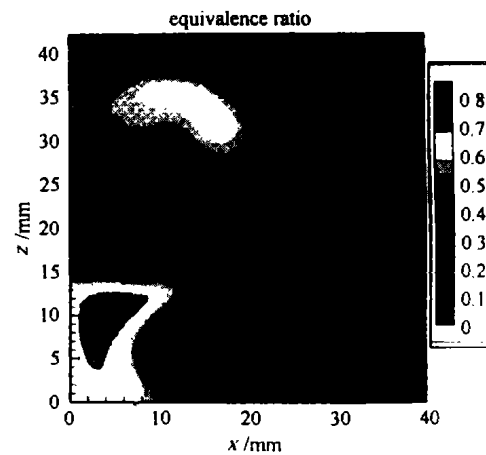


Fig. 11 Contours of NG-air equivalence ratio in the exhaust at $t = 767.86$

ence of injection with large speed can suppress the boundary layer separation happening at the top wall due to the channel expansion, but makes the

near wake flow more complicated. The mixing region can be widened by increasing the injection velocity.

The recurrence of the vortex structure and the coherent structure can be found from the full N-S simulation. It can be concluded that increasing the injection velocity can improve the effectiveness of mixing of NG and air in the near wake of the injectors.

ACKNOWLEDGEMENT

This work was supported by the Technical Center of Diesel Engines of Shanghai Limited Corporation. The authors thank Prof. XU Li-gong at USTC for useful discussion.

REFERENCES

- [1] GIPTA M. , BELL S. R. and TILLMAN S. T. Investigation of lean combustion in a natural gas-fueled spark-ignited engine[J]. **ASME Journal of Energy Resources Technology**, 1996, 118(2):145-151.
- [2] YUSAF T. F. , SHAMSUDDIN A. H. , ALI Y. and AHMAD F. Study of dual fuel system using compressed natural gas for commercial diesel engine[J]. **International Journal of Power and Energy Systems**, 1999, 19(2):163-167.
- [3] HILL P. G. and DOUVILLE B. Analysis of combustion in diesel engines fueled by directly injected natural gas [J]. **ASME Journal of Engineering for Gas Turbines and Power**, 2000, 122(1):141-149.
- [4] ROSEN J. Running on methane[J]. **Mechanical Engineering**, 1990, 112(5): 66-71.
- [5] PATANKAR S. V. **Numerical heat transfer and fluid flow**[M]. New York; McGraw Hill, 1980, 1-10.
- [6] BROWN D. L. CORTEZ R. and MINION M. L. Accurate projection methods for the incompressible Navier-Stokes equations[J]. **J. Computational Physics**, 2001, 168:464-499.
- [7] ZHU Zuo-jin and YANG Hong-xing. Numerical investigation of transient laminar natural convection of air in a tall cavity[J]. **Heat and Mass Transfer**, 2003, 39(7): 579-587.
- [8] LE QUERE P. and ROQUEFORT T. A. D. Computation of natural convection in two-dimensional cavities with Chebyshev polynomials [J]. **J. Computational Physics**, 1985, 57:210-228.
- [9] XIN S. H. , LE QUERE P. and TUKERMAN L. S. Bifurcation analysis of double-diffusive convection with opposing horizontal thermal solutal gradient[J]. **Physics of Fluids, A**, 1998, 10(4):850-858.
- [10] WANG Ya-ling, LIU Ying-zhong and MIAO Guo-Ping. Calculation of viscous flow around circular cylinder with three-dimensional numerical simulation[J]. **Journal of Hydrodynamics, Ser. B**, 2001, 13(4):83-87.
- [11] SHUEN J. S. Upwind Differencing LU factorization for chemical non-equilibrium Navier-Stokes equations[J]. **J. Computational Physics**, 1992, 99:233-250.
- [12] KNUPP P. M. , A robust elliptic grid generator[J]. **J. Computational Physics**, 1992, 100:409-418.
- [13] YU S. T. , TSAI Y. L. P. and SHUEN J. S. Three-dimensional calculation of supersonic reacting flows[J]. **J. Computational Physics**, 1992, 101:276-286.
- [14] YOON S. , JAMESON A. LU implicit scheme for high speed inlet analysis[R]. AIAA paper, AIAA-86-1520, 1986.
- [15] JAMESON A. , YOON S. , LU implicit scheme with multiple grids for the Euler equations[R]. AIAA paper. AIAA-86-0105, 1986.
- [16] JANAF THERMALCHEMICAL TABLES. Natinal Bureau of Standard Publication [R]. NSRDS-NBS37, 1971.
- [17] MONTAGNE J. L. , YEE H. C. , KLOPFER G. H. and VINOKUR M. Hypersonic blunt body computations including real gas effects[R]. NASS TM-10074, 1988.
- [18] AMSDEN A. A. , O'ROURKE P. J. , BITHER. T. D. Kiva-II; A computer program for chemically reactive flows with sprays[R]. LA11560-MS, 1989.